ACS Catal. 2016, 6, 3, 2076–2088 DOI: 10.1021/acscatal.5b02329

Inhibition of Xylene Isomerization in the Production of Renewable Aromatic Chemicals from Biomass-Derived Furans

C. Luke Williams[1,‡], Katherine P. Vinter[3,‡], Ryan E. Patet[2], Chun-Chih Chang[1], Nima Nikbin[2], Shuting Feng[2], Matthew R. Wiatrowski[2], Stavros Caratzoulas[2], Wei Fan[1], Dionisios G. Vlachos[2], Paul J. Dauenhauer[1,3*]

[1]Department of Chemical Engineering and Catalysis Center for Energy Innovation, University of Massachusetts, 686 North Pleasant Street, Amherst, MA 01003, USA.
[2]Department of Chemical Engineering and Catalysis Center for Energy Innovation, University of Delaware, 150 Academy Street, Newark, DE 19716, USA.
[3]Department of Chemical Engineering and Materials Science, University of Minnesota, 421 Washington Ave. SE, Minneapolis, MN 55455, USA.
*Corresponding Author: hauer@umn.edu
‡Authors contributed equally.

Keywords: Isomerization, xylene, zeolite, dimethylfuran, Diels-Alder, furan

Abstract. Inhibition of *p*-xylene isomerization in the presence of H-Y (Si/Al 2.6) and H-BEA (Si/Al 12.5) zeolites was studied under conditions relevant to *p*-xylene production from 2,5-dimethylfuran (DMF) and ethylene. Through examination of the reaction components present in the highest concentrations, it was shown that both DMF and 2,5-hexanedione inhibit transalkylation and methyl shift reactions of *p*-xylene, while other reaction components, water and ethylene, do not. Retention of Brønsted acid sites after reaction was shown through the use of ^{27}Al-NMR for both H-Y and H-BEA zeolites, but with a reduction in the ratio of tetrahedrally-coordinated aluminum (strong acid sites) to octahedrally coordinated aluminum (Lewis acid sites) coinciding with the disappearance of the framework aluminum. Diffuse reflectance spectroscopy has shown preferential adsorption of DMF and 2,5-hexanedione (DMF+H_2O) relative to *p*-xylene to the Brønsted acid sites located in the super and sodalite cages of the H-Y. Desorption characteristics for DMF and *p*-xylene in H-Y and H-BEA were determined by thermogravimetric analysis, consistent with adsorption energetics of individual chemical species and dimeric complexes evaluated by the ONIOM method. Evaluation of three mechanisms allowing for production of *p*-xylene from DMF and ethylene while also inhibiting *p*-xylene isomerization supports high surface coverage of the active site with 2,5-hexanedione, supported by electronic structure calculations.

1. Introduction. Production of biorenewable fuels and chemicals has gained interest due to an increased demand for energy independence and the need for sustainable products and materials.[1,2] Initial approaches to renewable fuels and chemicals have focused on enzymatic or hybrid enzymatic/thermochemical processing of biomass for renewable fuels and chemicals.[3] A hybrid process combines the benefits of high selectivity provided by enzymes and the speed of thermochemical processes. A third option utilizes highly selective inorganic catalysts, such as supported metals or oxides, for a thermochemical process to produce furans and other basic chemicals from biomass-derived sugars.[4,5] One renewable chemical of interest is *p*-xylene, which can be directly integrated into modern chemical platforms for the production of PET, a material used in multiple consumer products such as plastic bottles.[6,7] In addition, consumption of benzene/toluene/xylenes (BTX) continues to aggressively grow and could be offset with biomass sources.[8]

Thermochemical production of *p*-xylene from sugars benefits from a limited number of reactions, each of which can be independently optimized to high selectivity for an overall process with viable yield. Isomerization of glucose to fructose occurs using biological (i.e., enzymes) or thermochemical catalysts, including base catalysts[9] and Lewis acid heterogeneous catalysts, such as Sn-Beta.[10] Fructose then dehydrates to hydroxymethylfurfural[11], which is further hydrodeoxygenated to produce 2,5-dimethylfuran (DMF).[12] The last step produces *p*-xylene from DMF and ethylene (itself produced by dehydration of ethanol), which completes the transformation of renewable biomass feedstock to aromatic chemicals and can be integrated within existing refinery infrastructure.[13-15]

Initial studies of the final step of furan conversion to aromatic chemicals with six-carbon rings have demonstrated high selectivity (75-90%) to *p*-xylene from DMF using H-Y and H-BEA zeolites[14] and have stimulated further research on the process chemistry, kinetics and catalytic mechanisms. Experimental examination of the reaction pathways of cycloaddition of ethylene/DMF identified three competing reactions: (a) hydrolysis of DMF, (b) multiple addition of ethylene to DMF to form alkylated aromatic chemicals, and (c) dimerization of furans.[14] Additionally, gas-phase DFT has evaluated the series mechanism of Diels-Alder cycloaddition of ethylene/DMF combined with dehydration to produce *p*-xylene.[15,16] These studies highlighted the capability of Brønsted acidity to catalyze the dehydration of the Diels-Alder cycloadduct (oxanorbornene intermediate), the overall rate-limiting reaction absent catalysts. Further calculations have identified the beneficial role of Lewis acids like lithium, which can potentially lower the energy barrier of cycloaddition and increase the overall reaction rate.[15,16]

Despite progress on development of thermochemical conversion of DMF to *p*-xylene, there remain several important aspects of the reaction that are not well understood. One of the main benefits of this process is its high yield to xylenes as well as its extremely high stereo-selectivity (99%) to the *para*-isomer of xylenes; this particular attribute nearly eliminates the need for expensive xylene separation.[17] It is well known that *ortho*-, *meta*- and *para*-xylenes readily isomerize in the presence of solid acid catalysts, such

as H-Y and H-BEA zeolite, under the reaction temperatures of 240 to 300 °C.[18-22] However, isomerization and transalkylation have not been observed during the production of *p*-xylene from DMF using H-Y or other solid acid catalysts; once formed, *p*-xylene remains intact.[14,15]

Isomerization of xylenes occurs through both intramolecular and intermolecular pathways in zeolite catalysts. The unimolecular mechanism proceeds through a 1,2-methylshift, allowing for reactions such as a shift of *p*-xylene to *m*-xylene. Alternatively, the bimolecular mechanism can occur through transalkylation, requiring two adjacent acid sites, to form toluene and trimethylbenzenes (TMB) from *p*-xylene.[19] The favored isomerization mechanism depends on reaction conditions and catalyst properties including temperature, catalyst microstructure, acid site density and acid site strength. The bimolecular mechanism is more favored in zeolites than in catalysts like silica-alumina[19] as well as at higher temperatures, as it requires 3-4 kcal/mol more energy than the unimolecular mechanism.[20] The bimolecular pathway, associated with disproportionation on adjacent acid sites, is favored in zeolites as the Si/Al ratio decreases (greater Brønsted acid site density), and the pore size of the zeolite increases.[21,25-27] Considerations of reaction temperature, and the greater acid site density in zeolites, indicates that the bimolecular mechanism, which produces toluene and trimethylbenzene, should occur when producing *p*-xylene from DMF using H-Y and H-BEA zeolite.[21]

The role of strong acid sites within H-Y and H-BEA for catalyzing dehydration of Diels-Alder cycloadducts of furans, while not promoting isomerization, is of primary interest. Characterization of zeolite structure and acid sites, and in some cases elucidation of species bound to them, has been achieved through FT-IR.[22-24] Siliceous faujasite contains a characteristic peak associated with the external silanols located at 3743 cm^{-1}. Additionally, characteristic peaks for the tetrahedrally-coordinated strong acid sites in the supercages and sodalite cages are located at 3627 cm^{-1} and 3563 cm^{-1} respectively.[23] Characterization of these acid sites has been complemented by ^{27}Al MAS NMR, which monitors type and relative ratio of acid sites in faujasite and beta.[22,24,25] In the case of dealuminated H-Y zeolite, tetrahedrally coordinated aluminum, denoted by an NMR frequency shift of ca. 60 ppm, represents strong Brønsted acid sites. Octahedrally coordinated aluminum denotes extraframework aluminum, represented by a peak at ca. 0 ppm, which is slightly Lewis acidic.[22] In the case of dealuminated H-Y, there also exists a peak shoulder at ca. 32 ppm, which has been previously attributed to distorted tetrahedrally coordinated aluminum.[26 27] ^{27}Al-NMR of H-BEA shows a similar spectrum to that of H-Y and has tetrahedrally coordinated Al at 60 ppm and octahedrally coordinated Al at 0 ppm. The capability for xylene isomerization is dependent on the concentration of these acid sites before, during and after reaction.

This paper characterizes the acid sites of zeolites used in Diels-Alder cycloaddition and subsequent dehydration of DMF/ethylene and investigates the mechanism leading to inhibition of *p*-xylene isomerization in H-Y and H-BEA zeolites. Inhibition is evaluated by considering xylene isomerization in

the presence of the most prevalent components in the reaction of DMF with C_2H_4. The interaction of chemical adsorbates with active sites was examined by diffuse reflectance infrared fourier transform spectroscopy (DRIFTS) to establish the preferential adsorption of 2,5-hexanedione (hydrolysis product of DMF) versus *p*-xylene on strong Brønsted acid sites. Acid sites were quantitatively characterized before and after use by isopropylamine TPD; additional characterization utilized ^{27}Al-NMR to determine the extent of structural transformation of zeolite acid sites before and after reaction. Finally, thermogravimetric analysis (TGA) provided insight into the degree of cationic polymerization of DMF present on the strong acid sites present in the faujasite.[27, 32]

Based on experimental observations, three potential hypotheses were investigated computationally to explain the observed inhibition of *p*-xylene isomerization. To test the first mechanism of individual components blocking strong acid active sites (i.e. high surface coverage), adsorption energies were calculated with an ONIOM model of H-Y zeolite framework. In a second mechanism, co-adsorption of the reaction components in the system were also measured in the H-Y ONIOM model, to evaluate whether the adsorption of multiple adsorbates (e.g. pie-stacked xylenes or DMF) could be blocking the active site with high surface coverage. Additionally, a third proposed mechanism was evaluated to test the ability of the zeolite framework to transfer a proton to the reactive adsorbates mediated by adsorbed dimethylfuran. These combined experimental and computational results serve to shed light on the processes which prevent the isomerization of *p*-xylene in Brønsted acid zeolite systems, leading to further improvement of a catalytic reaction system for the production of renewable chemicals.

2. Methods. Experiments focused on the isomerization of *p*-xylene in batch/semi-batch stirred pressure vessels. Additional characterization of adsorbates on H-Y and H-BEA zeolites utilized FT-IR, thermogravimetric analysis (TGA), and ^{27}Al-NMR.

2.1 Materials. Zeolites H-Y (CBV-600) and NH_4-BEA (CP814E) were obtained from Zeolyst with Si/Al ratios of 2.6 and 12, respectively. Zeolite Beta was calcined in flowing air at 550 ºC for 12 hours to achieve the H-BEA form. Acid site characterization using isopropylamine TGA-TPD yielded Brønsted site concentrations of 0.33 and 0.64 mmol(g)$^{-1}$ for H-Y and H-BEA, respectively[27]. Chemicals were purchased from Alfa Aesar and Sigma Aldrich at 98% purity or higher and used as received. All gases were purchased from Middlesex Gas Company at Ultrahigh Purity (UHP) or, in the case of air, grade 5.0.

2.2 Isomerization Reactions. Reactions to investigate the isomerization of *p*-xylene were conducted in a 160 mL stirred pressure vessel manufactured by Parr Instruments (model 4566B) with a 4848 controller and gas entrainment impeller. Temperature was maintained at 300 °C for all experiments, and gas pressure was maintained at 56.25 atm (800 psi). Samples were collected at pressure during the reaction using a double block sampling system described in Supplementary Figure S1. Nitrogen was used to pressurize all

reactions except for the investigation of ethylene as a potential inhibitor of isomerization. Catalyst loading was ~0.42 g (100 mL)$^{-1}$ of either H-Y or H-BEA). A typical reaction mixture consisted of 86 mL n-heptane (Alfa Aesar 99+%) and 2 mL tridecane (Sigma-Aldrich 98+%) as an internal standard with varying amounts of *p*-xylene (Alfa Aesar 99+%), 2,5-dimethylfuran (Alfa Aesar 98+%), and 2,5-hexanedione (Alfa Aesar 98+%), depending on the inhibition property tested. All chemicals were used without further purification.

Characterization of chemical components within the reaction mixture was performed with an Agilent 6890 gas chromatograph equipped with a G1513A autosampler, HP-Innowax column (to achieve separation of *o*,*m*,*p*-xylene isomers), and a flame ionization detector. Samples were collected under reaction conditions at high temperature and pressure. Details of the sampling system and procedure are described in Supporting Information[†]. Major species were identified by matching retention times with pure standards, and all reported data exhibited carbon balance closure greater than or equal to 90 C%.

2.3 FTIR Spectroscopy. FTIR analysis was performed with a Bruker Equinox 55 FT-IR spectrometer equipped with a Praying Mantis diffuse reflection attachment and high temperature reaction cell (Harrick). The spectra were recorded using a MCT detector with 2 cm^{-1} resolution and 128 scans. Helium flowed through the sample cell at 20 mL/min, providing an inert atmosphere. A KBr background was collected and subtracted from all samples. H-Y zeolite was degassed at 550 °C for one hour after a temperature ramp of 5 °C (min)$^{-1}$ from the starting temperature of 120 °C. The degassed zeolite was then saturated with the chemical of interest (DMF, *p*-xylene, or a 1/50th mixture of DMF/*p*-xylene) at 120 °C. Saturation of the catalyst was achieved through the use of a bubble column attached in line with the helium purge that maintained an inert atmosphere over the sample. The sample chamber was then heated to the upper range of reaction temperatures, 300 °C, for one hour to remove any weakly adsorbed chemicals before being cooled back to 120 °C for spectral acquisition.

2.4 Thermogravimetric Analysis (TGA). TGA samples were prepared by loading a ceramic cup with zeolite, heating to 550 °C at a temperature ramp rate of 10 °C (min)$^{-1}$, and holding for one hour to degas the sample. A constant helium purge of 23 mL (min)$^{-1}$ was passed through the furnace chamber to maintain an inert atmosphere. After the zeolite was degassed and cooled to 120 °C, DMF or *p*-xylene was added by redirecting the helium purge stream through a bubble column filled with the chemical of interest. Once the zeolite was saturated, the system was switched back to pure helium flow and any physisorbed species were removed. A temperature ramp of 10 °C (min)$^{-1}$ to 300 °C, with a one hour hold at that temperature, was then used to remove as much adsorbed material as possible at the maximum temperature.

2.5 Solid-State NMR. Solid-state ^{27}Al MAS NMR was used to investigate the aluminum content in H-Y and H-BEA zeolites before and after reaction. ^{27}Al MAS NMR spectra were recorded in a fully hydrated state with a Bruker DSX-300 NMR spectrometer at a ^{27}Al frequency of 78.2 MHz, using a 7 mm MAS probe. The spinning rate was 3 kHz and spectra were acquired with 0.5 s repetition time, 3 μs delay

time, and 2000 scans. The chemical shift was referenced to 1.0 M aqueous solution of $Al(NO_3)_3$ (0 ppm). The spectra taken prior to reaction was of unused zeolite (H-Y and H-BEA) labeled as "fresh" while the "spent" catalyst was used to produce *p*-xylene from DMF and ethylene at 300 °C in n-heptane solvent.

2.6 Calculation Methods. Heats of adsorption were computed using a mechanically embedded cluster model, which was treated with a hybrid quantum mechanics/molecular mechanics Hamiltonian within the ONIOM[28] method, as implemented in Gaussian 09.[29] The entire system, H-Y zeolite framework and adsorbates, was divided into three layers, which were treated at different theory levels. The first, inner, layer is the smallest of any adsorbates present in the system, consisting of 13 tetrahedral silicon atoms in the first two tetrahedral coordination spheres surrounding the aluminum atom. This layer was allowed to relax at all times and was treated quantum mechanically at the M06-2X/6-311G(2df,p) theory level. The second, medium, layer contains 16 tetrahedral silicon atoms in the third coordination sphere of the aluminum atoms and was also treated quantum mechanically, albeit at a lower theory level, M06-2X/3-21G, viz., with the same functional but smaller basis set. The M06-2X functional was used throughout this study in order to capture dispersion interactions between the zeolite and the adsorbate molecules[30]. The third, outer, layer consists of 188 tetrahedral silicon atoms in the next four coordination spheres of Al and was treated empirically with the Universal Force Field. Because optimizations with the medium and low layers fully relaxed were numerically unstable, the atoms of those layers were frozen at their crystallographic positions. The heats and free energies of adsorption were referred to as isolated species in heptane solvent, modeled using the SMD model; water adsorption was referred to as free water molecules in an implicit water solvent. The inner layer contribution to the binding energy has been corrected for the basis set superposition error using the counterpoise method. Gas-phase proton affinities reported in Figure 8 were calculated at the M06-2X/6-311G++(3df,3pd) theory level. All ground state and transition state geometries identified in this study were verified by vibrational frequency analysis.

3. Results. Inhibition of *p*-xylene isomerization was investigated primarily through the addition of different reaction components in a stirred pressure vessel, in the presence of H-Y and H-BEA zeolites. Analytical techniques including DRIFTS, TGA, and ^{27}Al-NMR provided insight on the key species bound to Brønsted acid sites, which are responsible for the inhibition of *p*-xylene isomerization. Finally, experimental results were compared with calculated adsorption enthalpies of reactants, products and intermediates.

3.1 Isomerization inhibition by principal reaction components. During production of *p*-xylene from DMF and ethylene, negligible *o*/*m*-xylene isomers were produced, despite the existence of acidic active sites capable of promoting isomerization of *p*-xylene.[14,15] To investigate the absence of isomerization products, the reaction of *p*-xylene was evaluated at conditions relevant to its production from DMF (i.e.

300 °C in n-heptane solvent using H-Y zeolite, CBV-600). As shown in supplementary Figure S2A[†], a reaction mixture of *p*-xylene in heptane with zeolite catalyst exhibited the expected behavior of rapid xylene isomerization; a significant portion of the *p*-xylene disproportionated and isomerized before reaching an asymptotic value of 55% conversion. Rearrangement of *p*-xylene produced numerous products, including *meta* and *ortho* xylenes as well as toluene, trimethylbenzene, and heavier alkylation products. Deactivation of the catalyst with time prevented the system from achieving equilibrium, which would result in a 2:1 ratio of *meta* to *ortho* and *para* xylene.[18] Catalyst deactivation was confirmed by performing a second experiment with increased catalyst loading, leading to increased conversion of *p*-xylene, as shown in Figure 1A. The increase in extent of reaction to 75%, as compared to Figure S2A, indicates that the system does not reach equilibrium before the catalyst deactivates at the lower catalyst loading.

To determine the source of xylene isomerization inhibition, the principal reaction components were tested individually for their impact on isomerization chemistry. The examined compounds include reactants DMF and ethylene as well as the most prevalent side products, 2,5-hexanedione and water. Co-feeding DMF was shown to strongly inhibit isomerization of *p*-xylene, as shown in supplementary Figure S3A. In a mixture that contained initial concentrations of 0.2 M DMF and 1.0 M *p*-xylene, no conversion of *p*-xylene was observed within experimental error. In a second experiment, reducing the initial DMF concentration by an order of magnitude (to 0.02M DMF) limited the isomerization of *p*-xylene to less than 5%, as shown in Figure 1B. The conditions shown in Figure 1B represent ten dimethylfuran molecules per Brønsted acid site for H-Y (Si/Al 2.6). This indicates that inhibition of xylene isomerization will occur even when *p*-xylene is present at concentrations fifty times greater than the DMF. For comparison with the original process of Scheme 1, this condition (*p*-xylene concentration fifty times DMF concentration) is the equivalent to 98% conversion of the dimethylfuran with 100% selectivity towards *p*-xylene. It can also be seen in Supplementary Figure S3C and Figure 1C that co-feeding DMF will inhibit *p*-xylene isomerization in the presence of H-BEA with results that are indistinguishable from those obtained for H-Y for both high and low DMF loadings. However, it should be noted that in both of these cases there is also 2,5-hexanedione, formed from hydrolysis of DMF with water adsorbed on the catalyst surface during heating, present in solution at amounts from one to two hexanedione molecules per Brønsted acid site.

The second chemical examined for inhibition of *p*-xylene isomerization was 2,5-hexanedione, the hydrolysis product of dimethylfuran. As shown in Figure 1D and Supplementary Figure S4A, isomerization of *p*-xylene was strongly inhibited by the presence of 2,5-hexanedione, exhibiting negligible *p*-xylene conversion within experimental error. Supplementary Figure S4A shows inhibition of *p*-xylene isomerization under conditions where the hexanedione concentration was set at one-fifth that of *p*-xylene (2 mL 2,5-hexanedione, 10 mL of *p*-xylene, and 88 mL of heptane solvent). Figure 1D depicts a reduction of hexanedione concentration by an order of magnitude to one fiftieth that of the *p*-xylene; in this case,

there were approximately ten hexandione molecules per Brønsted acid sites and conversion of *p*-xylene was still below 5%. This set of experiments shows that the conversion of the xylene will be inhibited to the same degree, for the considered conditions, with both 2,5-hexanedione and DMF.

While conducting experiments with results depicted in Supplementary Figure 4A and Figure 1D, it was observed that DMF and water were formed through acid-catalyzed cyclization of 2,5-hexanedione. The presence of DMF in the reaction mixture was particularly visible in Supplementary Figure S4A, where the concentration of DMF was far greater than hexanedione. This acid catalyzed cyclization has been observed to take place in high Al content H-ZSM5 at yields above 95%[31], which is consistent with our observations. Due to the cyclization reaction, the role of 2,5-hexanedione on *p*-xylene isomerization chemistry cannot be independently determined.

The final two chemical components examined were ethylene, the dienophile in the Diels-Alder cycloaddition reaction with DMF, and water, the product of cycloadduct dehydration. In the experiment shown in Figure 1E, *p*-xylene (12 mL) in heptane (86 mL) was reacted at 300 °C with 200 psi partial pressure ethylene (800 psig total, heptane vapor pressure). The addition of ethylene resulted in an increase in the number of heavily alkylated products and demonstrated no effect towards inhibiting isomerization of *p*-xylene. These heavily alkylated species constituted a wide array of products, the precise identification of which is outside the scope of this work. Addition of water reduced the rate of *p*-xylene isomerization, however the effect was minimal. As shown in Figure 1F, the reaction of 10 mL of *p*-xylene, 2 mL of water, and 86 mL of heptane was examined at 300 °C in the presence of H-Y zeolite. In both cases, the experiments achieved 60% *p*-xylene conversion and toluene and trimethylbenzene were observed as the dominant products at 60% selectivity.

3.2 Investigation of Brønsted acid sites. Figure 2A shows the ^{27}Al MAS NMR spectra of fresh and spent H-Y catalyst. Fresh catalyst was used as received. 'Spent' catalyst was used in the reaction of DMF (15 wt%) and ethylene (13.6 atm partial pressure) in heptane solvent at 300 °C. From the spectra of fresh H-Y catalyst, there exists a small amount of non-framework, pentacoordinated aluminum (32 ppm) in addition to framework tetrahedrally coordinated aluminum (60 ppm) and extraframework octahedrally coordinated Al (0 ppm). In comparison, the spectrum of spent catalyst does not exhibit the shoulder at 32 ppm. Additionally, the ratio of tetrahedral to octahedral coordinated aluminum has markedly decreased, indicating that a partial loss of part of the Brønsted acidity with reaction may occur. Framework aluminum, which produces Brønsted acid sites, exists in the examined H-Y zeolite both before and after reaction despite the aforementioned changes. Figure 2B illustrates the ^{27}Al MAS NMR spectra of H-BEA and shows a similar loss in Brønsted acidity upon reaction. Interestingly, octahedrally-coordinated Al at 0 ppm nearly disappears after reaction, and the intensity of the tetrahedrally coordinated Al (53 ppm) is reduced.[50]

Binding of reactant species to Brønsted acid sites in H-Y zeolite was examined using Diffuse Reflectance Fourier Transform Infrared Spectroscopy (DRIFTS). As shown in Figure 3, the IR spectra of degassed H-Y zeolite identifies initial -OH bonds, including: (a) the external silanols on H-Y faujasite at 3743 cm^{-1}, and (b) the tetrahedrally coordinated aluminum corresponding to the -OH stretching bands from the acid sites located in the super and sodalite cages at 3628 cm^{-1} and 3565 cm^{-1}, respectively.[23] It is shown in Figure 3 that acid sites (3628 cm^{-1} and 3565 cm^{-1}) are completely covered at a moderate temperature of 120 °C by adsorbing DMF, *p*-xylene, or a pre-mixed solution of the two (1:50 DMF to xylene by concentration). After heating to 300 °C, the strong acid sites at 3628 cm^{-1} and 3565 cm^{-1} are not regenerated by desorption of the DMF or the DMF/*p*-xylene mixture. However, when the zeolite saturated with *p*-xylene is heated to 300 °C, the peaks associated with Brønsted acid sites were completely recovered. The loss of the OH stretching bands associated with the strong acid sites, even after heating the dilute DMF in *p*-xylene mixture, strongly indicates that DMF (or its hydrolysis product, 2,5-hexanedione) is the chemical species bound to those sites.

TGA was performed on H-Y and H-BEA zeolites, with adsorbed DMF or *p*-xylene, to characterize desorption of these components in the temperature range of 100-300 °C, as shown in Figure 4. Vaporized chemicals were adsorbed on zeolites at 120 °C and then heated to 300 °C with an inert atmosphere. DMF remained adsorbed on H-Y and H-BEA at temperatures as high as 300 °C, as shown in Figure 4A and 4B. The y-axis indicating the number of adsorbed DMF species per active site was calculated by dividing the moles of reactant adsorbed by the previously measured Brønsted acid site concentration, for the fresh catalyst, provided in Table 1. DMF initially adsorbed at a ratio of about 4:1 with Brønsted acid sites on dealuminated H-Y zeolite (Figure 4A), while it only adsorbed with a ratio of 2:1 for H-BEA (Figure 4B). As the temperature was increased from 120 to 300 °C, only 40% of the adsorbed DMF desorbed from H-Y, leaving a ratio of two DMF molecules per Brønsted acid site at reaction temperatures (Figure 4A). For H-BEA, only 30% of adsorbed DMF molecules desorbed, leaving a final ratio of one DMF per acid site under reaction conditions (Figure 4B). In comparison, *p*-xylene binds at a ratio of about 3:2 to Brønsted acid sites of both H-Y and H-BEA, as shown in Figure 4C and 4D, respectively. However, at a temperature of 120 °C under flowing helium, more than 50% of *p*-xylene desorbed from both zeolites. Upon heating to 300 °C, all of the *p*-xylene desorbed from H-Y and almost all from H-BEA (Figure 4C and D). TGA analysis was also performed on γ-alumina, a surrogate for the octahedrally coordinated Al in the zeolites, to gain an understanding of how DMF would desorb from Lewis acid sites. However, data presented in supporting Figure S6 shows that DMF readily desorbs from γ-alumina at a temperature of only 160 °C[†].

3.3 Enthalpy and Gibbs Free Energy of Intermediates and Energy Barriers in H-Y zeolite. Figure 5 depicts the adsorption geometry of dimethylfuran, *p*-xylene, 2,5-hexanedione, and 1,4-dimethyl-oxanorbornene on acids sites within the supercage of H-Y zeolite. Table 2 shows calculated single molecule

enthalpies and free energies of binding of DMF, *p*-xylene, oxanorbornene, hexanedione, water and ethylene with H-Y at 200, 250 and 300 °C. Both DMF and *p*-xylene exhibited similar heat of adsorption, $\Delta H_{ads} \approx$ -21 kcal/mol, at 300 °C. As expected, at high temperatures the negative entropy of adsorption dominates the Gibbs free energy change: at 300 °C, $\Delta G_{ads,\ DMF} \approx$ -2 kcal/mol and $\Delta G_{ads,\ pX} \approx$ -0.3 kcal/mol. Thus, for adsorption at a ratio of one molecule per active site, DMF and *p*-xylene adsorb competitively. Oxanorbornene and 2,5-hexanedione have stronger binding to acid sites within H-Y, $\Delta H_{ads} \approx$ -30 kcal/mol for both, which is not a surprising result considering that they are significantly more polar molecules than DMF and *p*-xylene. From an entropic point of view, the two molecules behaved similarly upon adsorption and thus their *relative* binding strengths do not change with temperature: $\Delta G_{ads,\ hxdn}$ = -8.5 kcal/mol, and $\Delta G_{ads,\ oxa}$ = -9.7 kcal/mol, at 300 °C. Thus, hexanedione, produced by Brønsted acid-catalyzed hydrolysis of DMF, can block the acid sites of the zeolite via stronger adsorption. Similar blocking of the active sites can take place in the presence of oxanorbornene, the product of Diels-Alder cycloaddition between DMF and ethylene. From the calculations of Table 2, both water and ethylene bind less strongly than *p*-xylene, in agreement with our observations that neither of the two has an inhibitory effect on the isomerization of *p*-xylene.

Bimolecular DMF-DMF and DMF-*p*-xylene co-adsorption was also investigated, with the calculated binding enthalpies and Gibbs free energies shown in Table 2 and depicted in Figure 6. Among the different adsorption configurations considered, two configurations were dominant, differing in the orientation of the molecular planes of the adsorbates relative to the plane of the H-Y Site II hexagonal prism. In the first geometry (P), the adsorbates were stacked with their planes parallel to the plane of the active site, with only one of them interacting directly with the Brønsted hydrogen atom. In the second geometry (T), both molecules interacted with the active site (albeit one more than the other), with their planes in a perpendicular arrangement relative to the plane of the active site.

For DMF-DMF adsorption, the (P) geometry was more stable than the (T) geometry by about 7 kcal/mol. Both configurations, however, were significantly more stable than only one DMF molecule at the active site, which is in agreement with our conclusions from the TGA experiments, namely, that, at 300 °C, DMF adsorbs at a ratio of two molecules per Brønsted acid site. The extra enthalpic stabilization is about 16 kcal/mol for the (P) configuration and 9 kcal/mol for the (T) configuration. DMF is an aromatic molecule and thus it is not surprising that, under confinement, the observed π-π stacking leads to the formation of a stable dimeric complex. Moreover, it is conceivable that, upon adsorption, the DMF-DMF dimer is benefited by an electrophile-nucleophile interaction – in both the (P) and (T) adsorption geometries, one of the two DMF molecules is in more direct contact with the Brønsted proton and thus an electrophilic character should be bestowed upon it, more so in the case of the (P) arrangement.

For DMF-*p*-xylene co-adsorption, the (P) geometry with DMF at the active site and *p*-xylene on top of DMF is slightly more stable than the (P) configuration with *p*-xylene instead of DMF at the active site, by about three kcal/mol. The (T) geometry was also stable, but somewhat less so than the most stable (P) geometry, by about five kcal/mol. Compared to DMF-DMF co-adsorption, DMF-*p*-xylene co-adsorption was slightly more favorable, but within the uncertainty of the calculations, one should conclude that they are both equally likely from a thermodynamic point of view.

When DMF was adsorbed at the active site, the Brønsted acid proton can facilely transfer to the α-C or β-C of the ring, requiring about 6.3 and 7.8 kcal/mol, respectively; transfer to the α-C was slightly more favorable thermodynamically (see Table 3). Direct proton transfer from H-Y to *p*-xylene at the active site was significantly slower and more endothermic, with free energies of activation and reaction equal to 18 and 16.7 kcal/mol, respectively. The protonated DMF-site complex could therefore serve as a new active site with reduced acidity.

DMF-mediated proton transfer from H-Y to *p*-xylene was investigated by considering the DMF-*p*-xylene complex in the (P) configuration with DMF at the active site. Our calculations (Table 3) show that this process is not only slower than direct proton transfer from H-Y to *p*-xylene, but also more thermodynamically unfavorable as the proton affinity of DMF exceeds that of *p*-xylene by about 17 kcal/mol. The activation free energy for proton transfer from protonated DMF to *p*-xylene was calculated at 27 kcal/mol, which, when combined with the activation energy for proton transfer from H-Y to adsorbed DMF, raises the overall activation energy to about 35 kcal/mol. Although an adsorbed DMF molecule can quite easily accept the Brønsted proton, it does not relinquish it as easily to *p*-xylene.

In contrast, a proton transferred from the zeolite acid site to adsorbed DMF can undergo a second abstraction to oxanorbornene. As depicted in Figure 7, a proton originating from the zeolite acid site and residing at the DMF β-carbon can be transferred to the oxanobornene oxygen bridge atom with an activation energy of E_a=9.8 kcal/mol. Following the proton transfer, the protonated and positively charged oxanorbornene can displace the intermediary DMF near the negatively charged zeolite aluminum site and proceed to dehydrate to *p*-xylene. As shown in Figure 7, the second transition state corresponds to the opening of the ether bridge (E_a=10.1 kcal/mol). The third transition state involves H^+ transfer from an ethylene moiety carbon atom to the oxygen atom (E_a=13.9 kcal/mol). *p*-Xylene formation ensues as the system passes through the fourth transition state (E_a=13.8 kcal/mol). Thus, DMF-mediated proton transfer could enable oxanorbornene dehydration to *p*-xylene while simultaneously blocking protonation of xylenes and subsequent isomerization (e.g. methyl shift chemistry) and transalkylation.

4. Discussion. Figure 1A illustrates that, as expected, *p*-xylene readily isomerizes in the presence of H-Y and H-BEA zeolites for the conditions that are required to produce it from DMF and ethylene (>200 °C) in

the method of Scheme 1. The existence of twice as much toluene and trimethylbenzene in the products as compared to *ortho*- and *meta*-xylene indicates that the predominant isomerization mechanisms are bimolecular in nature. Prevalence of the bimolecular reaction path is likely due to the high density of acid sites present in the considered zeolites, H-BEA (Si/Al 12.5) and H-Y (Si/Al 2.6).

While isomerization of *p*-xylene occurs with fresh zeolites, a first consideration for the mechanism leading to inhibition of *p*-xylene isomerization in the reaction of DMF and ethylene must consider that strong Brønsted acid sites are destroyed during reaction. Water produced in the production of *p*-xylene from DMF has the potential for converting strong acid sites in both H-Y and H-BEA to extraframework Lewis acid sites.[32] However, characterization of H-Y and H-BEA shown in Table 1 reveals that strong acid sites exist both before and after reaction. Additionally, from the ^{27}Al MAS NMR of Figure 2, the spectra of fresh and spent H-Y and H-BEA both indicate the presence of tetrahedrally-coordinated aluminum that comprises Brønsted sites at 60 and 50 ppm. The extraframework tetrahedrally coordinated aluminum acid sites associated with the peak at 32 ppm disappears for H-Y, but it has been previously noted that the extraframework Al associated with this peak is less stable and does not play a strong role in acidity[22]. Given the weak role in acidity of the peak at 32 ppm, it seems unlikely that the loss of this peak after reaction will greatly affect overall catalyst activity. Further evidence that strong acid site concentration is not significantly altered comes from previous work that shows identical activity for production of *p*-xylene from DMF for H-Y catalysts regenerated in flowing air at 550 °C.[14,15] It can be concluded that Brønsted acid sites remain in the zeolite catalysts before, after, and during reaction.

The absence of *p*-xylene isomerization in the reaction of DMF and ethylene indicates that a reactant (or intermediate/product) occupies the Brønsted acid sites necessary for xylene isomerization chemistry to occur. When DMF is added to the reaction mixture, conversion of *p*-xylene over the considered zeolites to xylene isomers or toluene/trimethylbenzene completely stops (Figure 1B-1D). This effect is particularly strong, as it occurs at low concentrations relative to *p*-xylene (1/50 DMF/*p*-xylene) as shown in Figure 1B. The inhibition effect also occurs with 2,5-hexanedione, a hydrolysis product of DMF; however it should be noted that DMF rapidly reforms through cyclization of 2,5-hexanedione, which is the thermodynamically favored chemical species in the presence of strong acid sites. In contrast, water and ethylene had no impact on the isomerization chemistry. These results indicate that DMF or 2,5-hexanedione adsorption on Brønsted acid sites is likely the key interaction of the inhibition mechanism.

Adsorption of DMF on strong acid sites was further studied through the use of DRIFTS, shown in Figure 3, allowing for monitoring of the Brønsted acid sites located in the super and sodalite cages (peaks at 3628 cm^{-1} and 3565 cm^{-1}, respectively). From this data, it is clear that DMF (or 2,5-hexanedione formed from DMF hydrolysis) remains adsorbed to strong acid sites at relevant reaction temperatures (200-300 °C), while *p*-xylene is completely removed upon heating. This effect is strong, as a mixture of 1/50th

DMF/*p*-xylene exhibits the same results as a saturated sample of pure DMF, providing strong evidence that DMF/hexanedione binds preferentially to Brønsted acid sites and blocks competing chemistries. Isomerization of *p*-xylene could also be occurring on the external surface of the zeolites, as well as in the micropores. It is possible that DMF/2,5-hexanedione covers these external sites to inhibit *p*-xylene isomerization.

TGA data provided in Figure 4A and 4B supports the strong binding of DMF (or its hydrolysis product, 2,5- hexanedione) to the Brønsted acid sites of H-Y and H-BEA zeolite, thereby inhibiting isomerization of the *p*-xylene. DMF inside H-BEA zeolite can be estimated at one molecule under reaction conditions and two molecules per Brønsted acid site for H-Y. Figure 4C and 4D also show that the majority of the bound *p*-xylene can be removed by flowing helium while holding at 120 °C before being completely desorbed upon heating to reaction conditions (T > 200 °C).

4.1 Active Site Adsorption of Reactant Species. Binding energies obtained from electronic structure calculations (Table 2) unexpectedly indicate that DMF and *p*-xylene bind equally well to H-Y acid sites, when adsorbed at a ratio of one molecule per active site. The heat of adsorption has previously been shown to correlate with proton affinity within H-form zeolites, which has been rationalized by a thermodynamic cycle such that the heat of adsorption (ΔH_{ads}) is comprised of three parts: (i) proton affinity of the zeolite, PA_{ZO^-}, (ii) proton affinity of the adsorbate, P_{AB}, and (iii) reaction of the adsorbate ion with the zeolite framework, $\Delta H_{binding}$.[33] By this methodology, molecules with high values of proton affinity such as 2,5-hexanedione (PA=213.2 kcal/mol), dimethylfuran (PA=206.9 kcal/mol) and the DMF-C_2H_4 cycloadduct (PA=206.2 kcal/mol) should have significantly higher heats of adsorption relative to *p*-xylene (PA=189.9 kcal/mol), water (PA=165.2 kcal/mol) and ethylene (PA=162.6 kcal/mol). Using proton affinities as a metric for heat of adsorption and predictor of surface coverage, it is anticipated that *p*-xylene has low surface coverage and low isomerization reaction rate. However, comparison of reactant/product proton affinities with computed heats of adsorption in Figure 8 reveal that the *linear* proton affinity prediction deviates below PA~200 kcal/mol. As proton affinity decreases, adsorbate/zeolite pairing transitions from an ion-pair interaction (linear with ΔH_{ads}) to a hydrogen-bonding interaction (non-linear with ΔH_{ads})[34]. Thus, while DMF and *p*-xylene have significantly different proton affinities, their calculated heats of adsorption are quite similar, as shown in Figure 8. Only 2,5-hexanedione and the DMF-ethylene cycloadduct have sufficiently high heats of adsorption to result in high zeolite surface coverage.

At the active site, another possibility is that the DMF molecule can form stable dimeric complexes either with another DMF molecule or with *p*-xylene, which could block acid sites, inhibiting *p*-xylene binding and isomerization. Calculated heats of adsorption listed in Table 2 for five combinations of DMF-DMF or DMF-*p*-xylene in both parallel (P) and perpendicular (T) stacking indicate strong binding, with ΔH_{ads} varying from about -40 to -30 kcal/mol, greatly exceeding the heat of adsorption of *p*-xylene (about

-21 kcal/mol). It is interesting to note that the enthalpy of complex formation (*p*-xylene-DMF or DMF-DMF) at the active site is lower than the total enthalpy of distributed adsorption of the corresponding monomers with a substrate to active site ratio of 1:1. This is due to the fact that, in the complex, the DMF molecule is interacting only weakly with the walls of the cavity, primarily via dispersion forces and more strongly with the *p*-xylene (DMF) molecule—especially in the (P) configuration via π-stacking. However, entropic losses due to binding have a significant effect on the free energies of binding. Thus, the free energy of complex formation is higher than the total free energy of distributed adsorption of the monomers. In the complex, the substrate molecule, which is not interacting directly with the active site, has more freedom of movement than if it were interacting directly with it. As a result, complex formation leads to reduced entropic losses than the distributed binding of the monomers. If we juxtapose binding of a dimeric complex with distributed 1:1 binding, then we see that at all temperatures shown in Table 2, formation of the *p*-xylene-DMF and DMF-DMF complexes is equally likely to distributed DMF binding at 1:1 ratio, within the accuracy of our calculations. At even higher temperatures, we expect that entropic contributions from individual 1:1 binding will grow faster than those for complex formation and thereby the latter will be somewhat favored. These conclusions hold irrespective of coverage, with the caveat that our model does not accurately capture high coverage lateral interactions for systems with low Si:Al ratio.

4.2 Mechanism of Isomerization Inhibition. The inhibition mechanism must be consistent with the reaction mechanism leading to production of *p*-xylene from dimethylfuran and ethylene. Specifically, blocking of xylene isomerization by DMF adsorption to Brønsted acid sites must still allow for dehydrative aromatization of oxanorbornene intermediates to six-carbon species, such as *p*-xylene. Three possible reaction mechanisms for *p*-xylene formation are considered, as depicted and summarized in Figure 9.

By the first mechanism, ethylene within the zeolite cage/pore could react directly with adsorbed DMF (green pathway of Figure 9), resulting in adsorbed oxanorbornene intermediate. Dehydration could then proceed via aromatization to desorbed *p*-xylene completing the catalytic cycle. However, in the ground state of active-site-bound DMF, the proton of H-Y has transferred to the α-C or β-C of the ring, breaking the conjugated π-system and thus eliminating the possibility for Diels-Alder chemistry. This reaction would then need to occur by stepwise addition of ethylene, as has been proposed for other reactions of furan.[35] However, stepwise addition of ethylene to DMF has been computed to be energetically unfavorable[15], making this mechanism unlikely to occur.

A second mechanism proposes that the DMF-Brønsted acid site complex forms a new, weaker Brønsted acid site. As drawn in Figure 9 (green pathway again), proton transfer from the H-Y zeolite Brønsted acid site to DMF can occur to the α-C, creating a DMF complex with an electrophilic furan α-carbon. A second proton transfer can then occur from the protonated α-carbon to the β-carbon of the adsorbed furan. DFT calculations, listed in Table 3, support this proton transfer, which is

thermodynamically favorable (ΔG = -3.3 kcal/mol) and does not require significant activation (E_a = 16.2 kcal/mol). The acidic β-C proton of the DMF complex may then be abstracted by the ether oxygen of a nearby oxanorbornene (formed homogeneously from DMF and ethylene). Once the proton on the β-C of the DMF-site complex is donated to the oxanorbornene intermediate, the previously adsorbed DMF molecule can be displaced at the active site by the newly protonated and strongly adsorbing oxanorbornene and dehydration can occur along the pathway illustrated in Figure 9. At the same time, although an adsorbed DMF molecule can quite easily accept the Brønsted proton of H-Y, it does not relinquish it as easily to *p*-xylene. The proton transfer process to *p*-xylene is thermodynamically unfavorable; the compounded activation energy for proton transfer from H-Y to DMF, and then to *p*-xylene, is about 35 kcal/mol. In summary, the second mechanism, whereby the acid site is the DMF-zeolite complex, indicates the formation of a new Brønsted acid site, which is sufficiently strong to protonate oxanorbornene, but sufficiently weak so as not to promote *p*-xylene isomerization.

The proposed second mechanism of acid sites consisting of DMF-Brønsted acid site complexes is consistent with TGA (Figure 4) and acid site titration results (Table 1). As shown in Table 1, H-BEA zeolites exhibit a loss in Brønsted acid site concentration upon reaction and calcination, reducing from 0.64 to 0.39$\pm$0.01 mmol/gram as determined by isopropylamine (IPA) titration. However, H-BEA zeolites that have been exposed to dimethylfuran exhibit the same number of Brønsted acid sites (0.42$\pm$0.01 mmol/g), indicating that the addition of dimethylfuran results in no significant change in the total number of strong acid sites present after reaction. In other words, the DMF-site complex is possibly titrated by IPA-TPD in the same manner as an exposed Brønsted acid site resulting from framework aluminum. Similar results were obtained with H-Y zeolite following quantification of Brønsted acid sites by IPA-TPD as shown in Table 1, but with a reduced total acid site density.

A third mechanism (blue pathway in Figure 9) considers the homogenous reaction of DMF and ethylene to form the Diels-Alder cycloadduct, followed by acid-catalyzed dehydration to *p*-xylene. According to the calculated binding energies, once the cycloadduct (ΔG_{ads}=-9.7 kcal/mol) is formed, either in the solution phase or in the zeolite pore/cage, it competitively adsorbs with DMF (ΔG_{ads}=-1.9 kcal/mol) or 2,5-hexanedione (ΔG_{ads}=-8.5 kcal/mol) on Brønsted acid sites at 300 °C and undergoes acid-catalyzed dehydrative aromatization, following a mechanism described in previous literature.[18,47] By this mechanism, the reaction conditions would need to exist such that the surface coverage of 2,5-hexanedione would be high to suppress *p*-xylene adsorption (ΔG_{ads}=-0.3 kcal/mol) and isomerization.

While the first mechanism is energetically unviable, evaluation of the second and third proposed mechanisms requires insight into the surface coverage to identify the reactant, intermediate, and/or product molecules occupying zeolite acid sites. We have recently conducted a simulation at the conditions of the reaction of dimethylfuran and ethylene utilizing the microkinetics of elementary Diels-Alder and

dehydration reaction steps obtained from first principles.[36,37] By varying the reactor conditions, it was shown that the overall reaction of dimethylfuran and ethylene could occur within two kinetic regimes: (a) overall rate limitation due to homogeneous Diels-Alder cycloaddition of DMF and ethylene, or (b) overall rate limitation resulting from zeolite-catalyzed dehydration of oxanorbornene. In either of the kinetic regimes, the resulting prediction of zeolite acid site surface coverages indicated that *p*-xylene negligibly occupied surface sites ($10^{-3}\% < \theta_{px} < 1\%$).[36] More importantly, the predicted surface coverages of zeolite acid sites indicates high coverage of 2,5-hexanedione for almost the entire extent of conversion of dimethylfuran with less than ~1% open sites (and less than 0.1% surface coverage of *p*-xylene). High coverage of dimethylfuran is only anticipated at the initiation of the reaction ($X_{DMF}<10\%$), where only small quantities of *p*-xylene have been produced. From this prediction, the third proposed mechanism of sight blocking (blue in Figure 9) would be the dominant method of inhibiting *p*-xylene. The second mechanism of DMF site blocking and proton-mediated dehydration by the pathway of Figure 9 could occur initially at low conversion at DMF.

4.3 Site-Blocking Compound: DMF Versus 2,5-Hexandione. Formation of 2,5-hexanedione by hydrolysis of DMF introduces additional complexity to identifying the mechanism resulting in inhibition of xylene isomerization. In the presence of water and acid sites, DMF will undergo ring opening to 2,5-hexanedione[38], and the reaction will rapidly achieve equilibrium.[16] According to the calculated binding energies, 2,5-hexanedione should adsorb strongly on Brønsted acid sites and the surface of H-BEA could be completely covered in hexanedione; inhibition could then result from site blockage by 2,5-hexanedione as previously discussed. For all considered reaction conditions of dimethylfuran and ethylene, water will be present allowing for formation of 2,5-hexanedione from DMF. At the start of the reaction, zeolites contain water which will react with DMF. Additionally, as the reaction of DMF and ethylene proceeds, water is formed as a major product. Additionally, in all considered experiments including the DRIFTS measurements of Figure 3 and the TGA measurements of Figure 4, the acidic zeolites will contain moisture from the air (even when experimental methods aimed to reduce these species), and 2,5-hexanedione will be produced. Thus, experimental and computational evidence supports the mechanism of high surface coverage of 2,5-hexanedione blocking xylene isomerization and transalkylation chemistry.

5. Conclusions. A combination of stirred vessel reaction experiments, spectroscopic measurements, DFT calculations and thermogravimetric analysis have been used to investigate the inhibition of *p*-xylene isomerization during production by the cycloaddition/dehydration of DMF and ethylene. The inhibition effect was shown to be strong, occurring at DMF/hexanedione concentrations as low as $1/50^{th}$ of *p*-xylene. No effect was observed from either water or ethylene. Use of ^{27}Al-NMR and isoproplyamine TGA has revealed that Brønsted acid sites exist in H-Y and H-BEA zeolites throughout the course of the reaction. In

addition, preferential binding of DMF/hexanedione over *p*-xylene to the strong acid sites in the super and sodalite cages of H-Y under reaction temperatures has been shown through the use of DRIFTS. Three mechanisms of xylene isomerization inhibition were considered: (a) strong DMF adsorption, (b) DMF-zeolite acid site complexes, and (c) strong adsorption of 2,5-hexanedione. The first mechanism was energetically unviable due to loss of diene functionality of DMF upon adsorption. The second mechanism was evaluated computationally, wherein the DMF-zeolite complex transfers an acidic proton from the β-C of the adsorbed DMF to the ether oxygen of a homogeneously-formed Diels-Alder cycloadduct (computed energy barrier of 8.4 kcal/mol). Subsequent dehydration to *p*-xylene was energetically favorable (Gibbs free energy -9.0 kcal/mol) while acid catalyzed isomerization of *p*-xylene by the DMF complex was shown to be energetically unfavorable. The third mechanism was supported by combined experiment and computation, which indicated strong adsorption of both 2,5-hexanedione and oxanorbornene (the DMF-ethylene cycloadduct). Comparison with a previously published microkinetic model indicated that the third mechanism of high surface coverage of 2,5-hexanedone is the dominant mechanism of xylene isomerization inhibition.

Associated Content

Supporting Information: Additional details about the FT-IR analysis, TGA/DSC data, and reaction system details are provided. This information is available free of charge via the internet at

Author Information

Corresponding Author
*Email: hauer@umn.edu

Acknowledgements

This work was supported as part of the Catalysis Center for Energy Innovation, an Energy Frontier Research Center funded by the U.S. Department of Energy, Office of Science, Office of Basic Energy Sciences under Award N. DE-SC0001004. This research used resources of the National Energy Research Scientific Computing Center, a DOE Office of Science User Facility supported by the Office of Science of the U.S. Department of Energy under Contract No. DE-AC02-05CH11231. The authors would like to acknowledge Zhoupeng Wang for his assistance in the collection of the Al-NMR data, Professor Raymond Gorte for helpful discussion of acid sites, and Geoff Tompsett for his helpful discussions about IR analysis and operation.

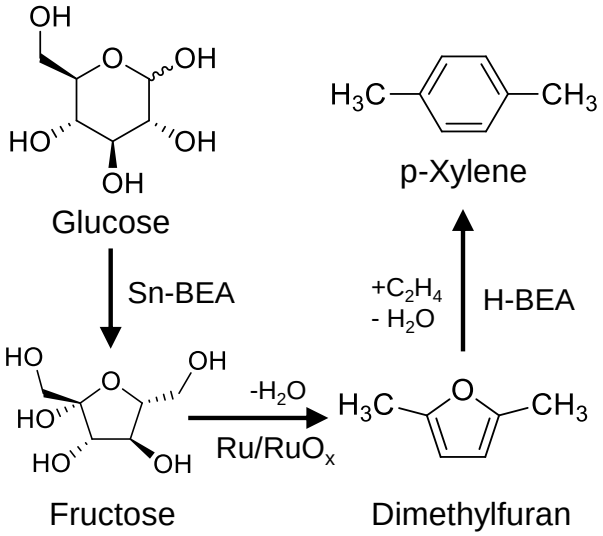

Scheme 1. Thermochemical Process to Convert Glucose to *p*-Xylene

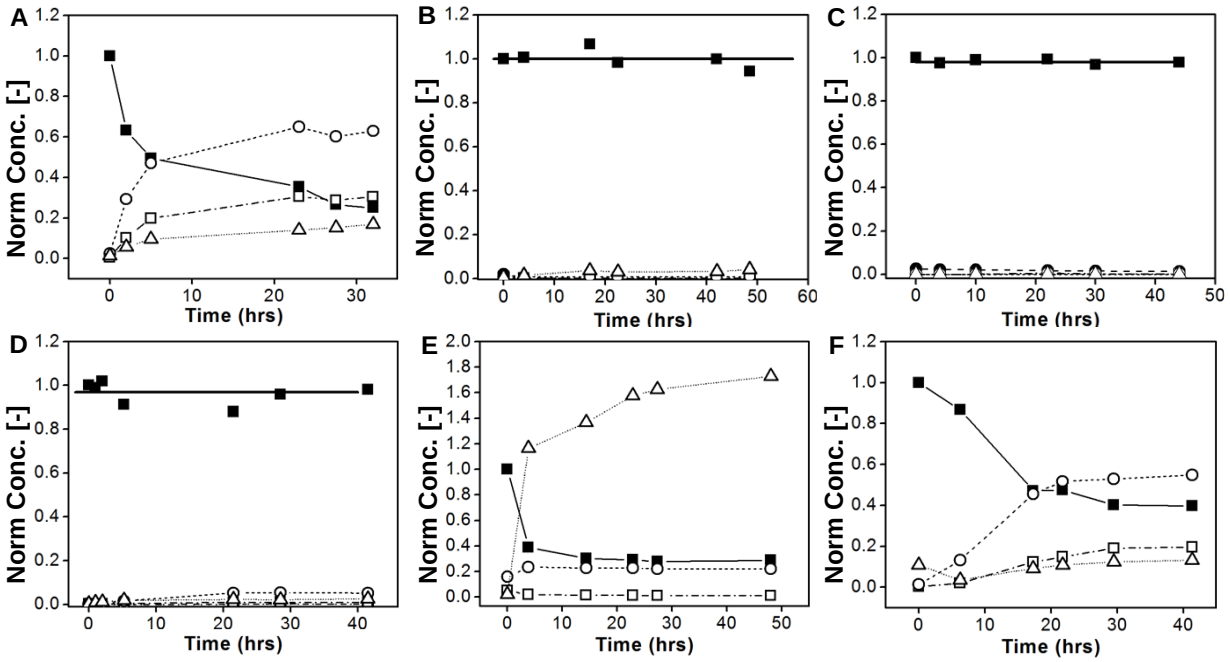

Figure 1. Inhibition of Xylene Isomerization via Chemical Site Blocking. Observed products include *p*-xylene (■), *o,m*-xylene (□), toluene and trimethylbenzene (○), DMF (●), hexanedione (▲), and alkylated products (△). **(A)** Isomerization of *p*-xylene readily occurs at conditions relevant to production of *p*-xylene from DMF and ethylene. Reaction Conditions: 300 °C, 800 psi N_2, 86 mL heptane, 12 mL *p*-xylene , 2 ml tridecane, 1.41 g H-Y Si/Al 2.6. **(B)** 2,5-Dimethylfuran inhibits isomerization reactions of *p*-xylene at 1/50th of the xylene concentration with 0.41 g H-Y zeolite Si/Al 2.6. Reaction Conditions: 300 °C, 54.4 atm (800 psi N_2), 86 mL heptane, 2 mL tridecane. **(C)** 2,5-Dimethylfuran inhibits isomerization reactions of *p*-xylene at 1/50th of the xylene concentration with H-BEA zeolite (Si/Al 12.5). Reaction Conditions: 300 °C, 54.4 atm (800 psi N_2), 86 mL heptane, 2 mL tridecane. **(D)** The presence of 2,5-hexanedione inhibits isomerization at 1/50th xylene concentration. Reaction Conditions: 300 °C, 54.4 atm (800 psi) N_2, 86 mL heptane, 2 mL tridecane, 0.41 g H-Y Si/Al 2.6, 12 mL *p*-xylene, 0.2 mL 2,5-hexanedione. **(E)** Ethylene promotes formation of heavy alkylated products in the presence of *p*-xylene in addition to isomerization products *o,m*-xylene. Reaction Conditions: 300 °C, 86 mL heptane, 2 mL tridecane, 0.42 g H-Y Si/Al 2.6, 54.4 atm (800 psi) ethylene, 12 mL *p*-xylene. **(F)** Water does not inhibit the isomerization of *p*-xylene. Reaction Conditions: 300 °C, 86 mL heptane, 2 mL tridecane, 0.42 g H-Y Si/Al 2.6, 54.4 atm (800 psi N_2), 10 mL *p*-xylene, 2 mL water.

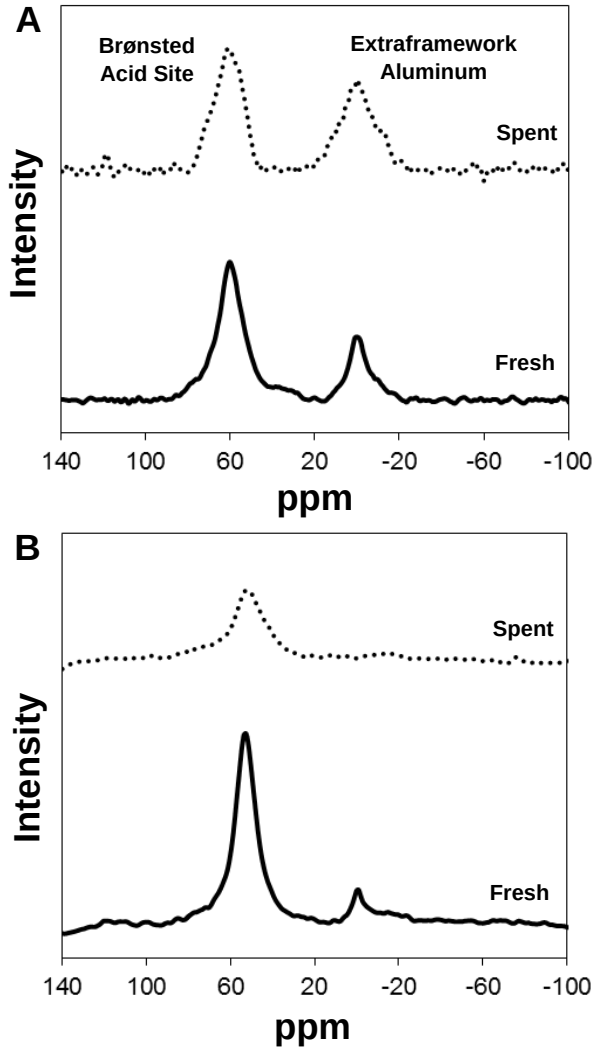

Figure 2. ^{27}Al-NMR of H-Y and H-BEA Zeolite. (A) H-Y zeolite (CBV600, Si/Al 2.6) used to produce *p*-xylene from DMF and ethylene and not regenerated by coke burnoff (spent) shows reduced tetrahedrally-coordinated aluminum (ca. 60 ppm) relative to octahedrally-coordinated aluminum (ca. 0 ppm) as compared to unused catalyst (fresh). (B) H-BEA zeolite (CP814E, Si/Al 12.5) used to produce *p*-xylene from DMF and ethylene and not regenerated by coke burnoff (spent) also exhibits reduced tetrahedrally-coordinated Al sites (60 ppm).

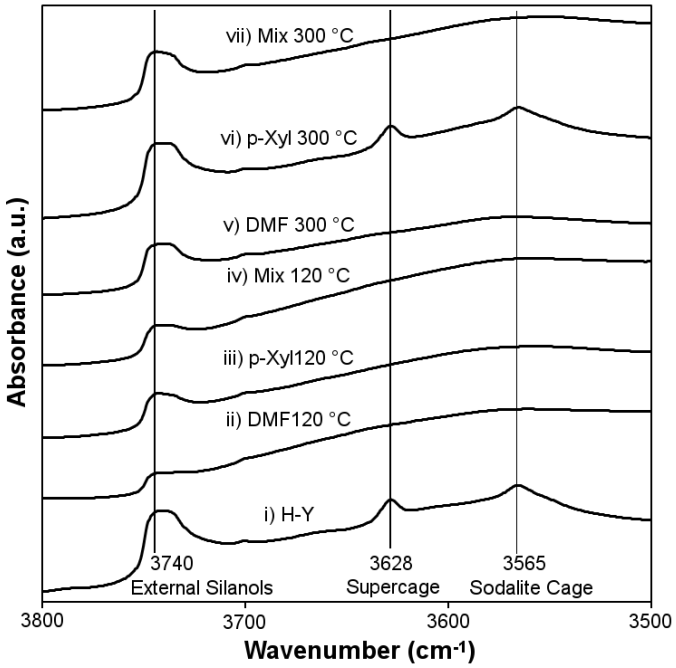

Figure 3. DRIFTS of DMF/*p*-Xylene on H-Y Zeolite. (i) Degassed zeolite H-Y (Si/Al 2.6) exhibits –OH stretches associated with external silanols (3740 cm^{-1}) and Brønsted acid sites in supercages (3628 cm^{-1}) and sodalite cages (3565 cm^{-1}). (ii-iv) Adsorption at 120 °C of DMF (ii), *p*-xylene (iii), and a 1/50 mixture of DMF/*p*-xylene (iv) shows absence of free Brønsted acid sites. (v-vii) Increasing the temperature to 300 °C recovers Brønsted acids previously occupied by *p*-xylene (vi), while DMF adsorbed on Brønsted acid sites associated within super- and sodalite cages remain adsorbed at 300 °C.

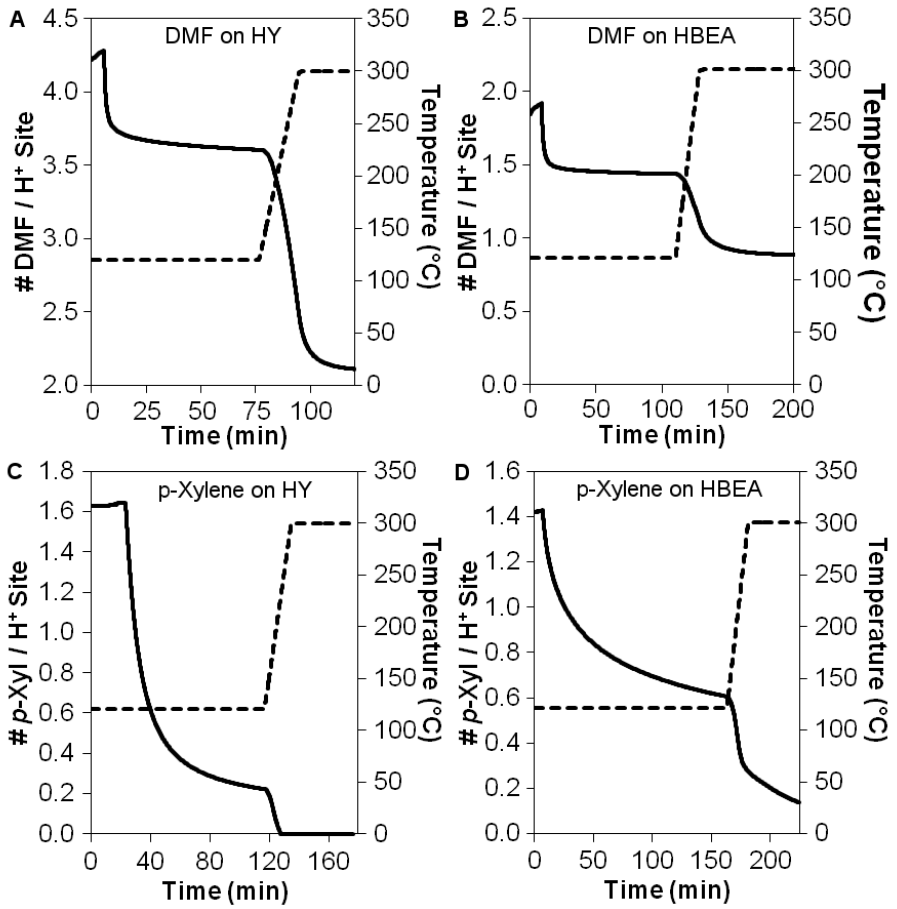

Figure 4. TGA of Adsorbed DMF and *p*-Xylene on H-Y (Si/Al 2.6) and H-BEA (Si/Al 12.5) Zeolites. Thermogravimetric analysis of 2,5-dimethylfuran (DMF) adsorbed on (A) H-Y and (B) H-BEA exhibits incomplete desorption. In comparison, TGA of *p*-xylene adsorbed on (C) H-Y and (D) H-BEA exhibits complete desorption at 300 °C.

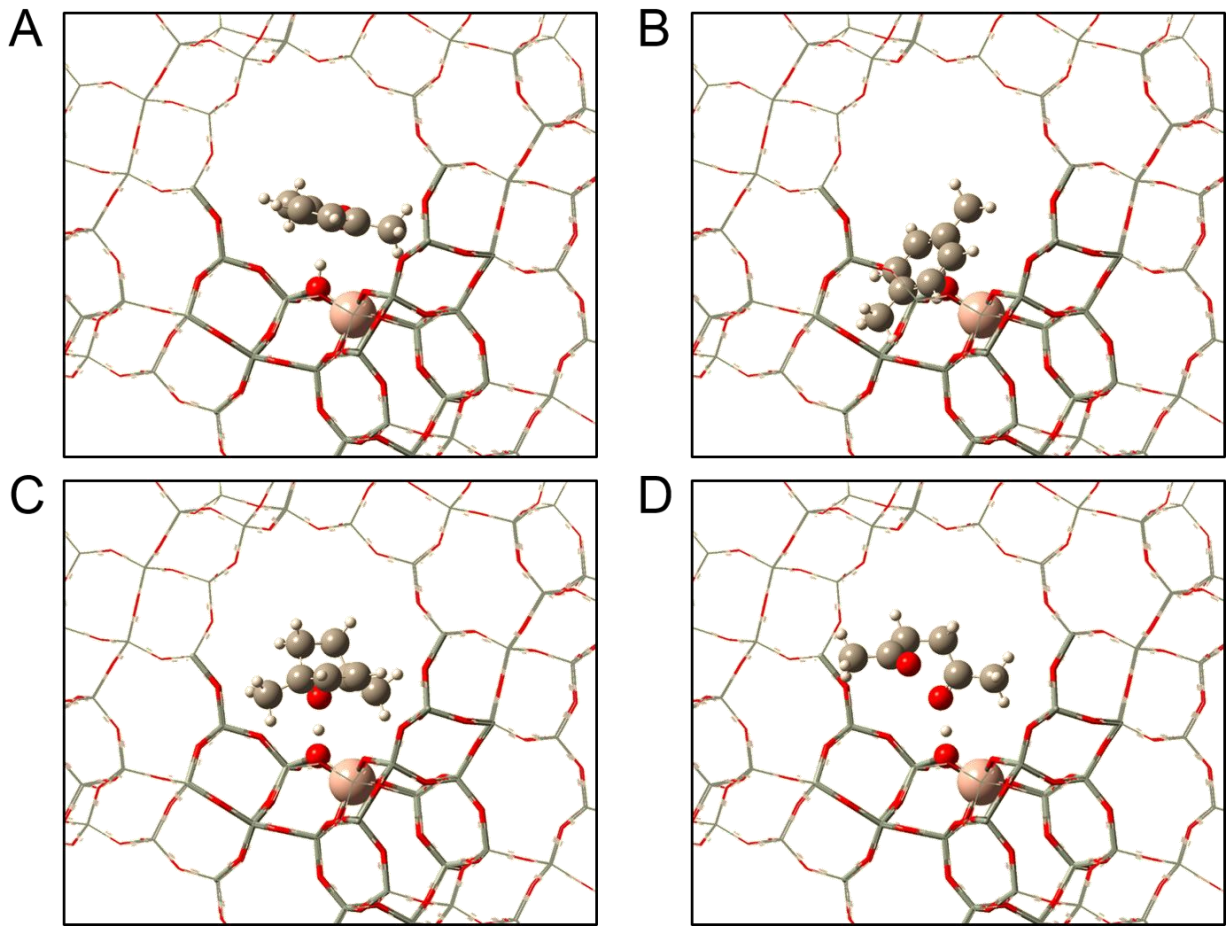

Figure 5. Single Molecule Binding Geometries at the HY Brønsted Acid Site. (A) 2,5-dimethylfuran, DMF. (B) *p*-xylene. (C) 1,4-dimethyl-oxanorbornene. (D) 2,5-hexanedione. (Note: Some of the ONIOM high-layer atoms have been merged into a medium layer, which is shown in the tube representation.)

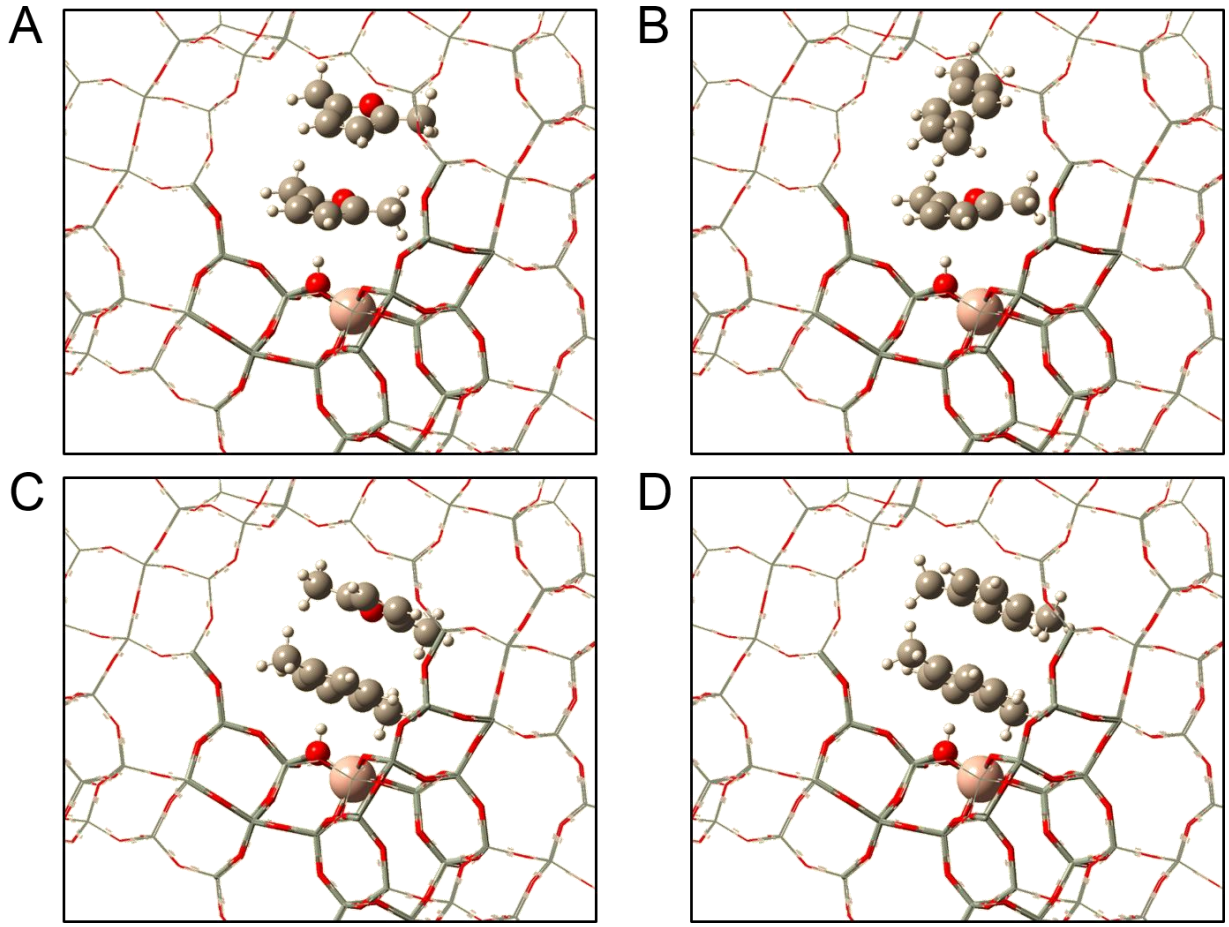

Figure 6. Binding geometries of dimeric complexes at the HY Brønsted acid site. **(A)** DMF-DMF, **(B)** DMF-*p*-xylene with DMF interacting with the active site, **(C)** *p*-xylene-DMF with *p*-xylene interacting with the active site, and **(D)** *p*-xylene-*p*-xylene. Only the most stable binding geometries are shown; molecules are stacked with their planes parallel to the plane of the hexagonal prism of HY Site II and with only one of the adsorbed molecules interacting directly with the Brønsted proton. (Note: Some of the ONIOM high-layer atoms have been merged into a medium layer, which is shown in the tube representation.)

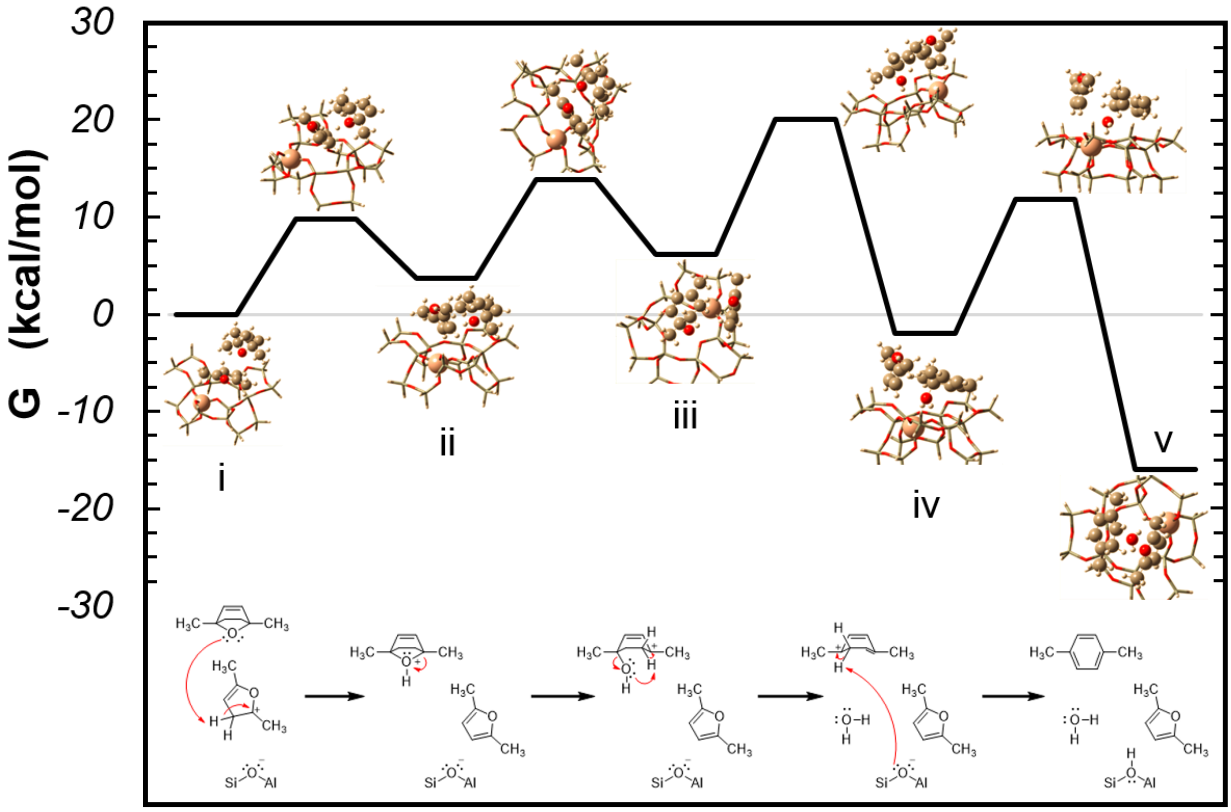

Figure 7. Free Energy Barriers for DMF-mediated proton transfer to the DMF-Ethylene Diels-Alder Cycloadduct and subsequent dehydrative aromatization. The first transition state involves H^+ transfer from the DMF β-C to the oxanorbornene oxygen atom (E_a=9.8 kcal/mol). The second transition state corresponds to the opening of the ether bridge (E_a=10.1 kcal/mol). The third transition state involves H^+ transfer from an ethylene moiety carbon atom to the oxygen atom (E_a=13.9 kcal/mol). *p*-Xylene formation ensues as the system passes through the fourth transition state (E_a=13.8 kcal/mol).

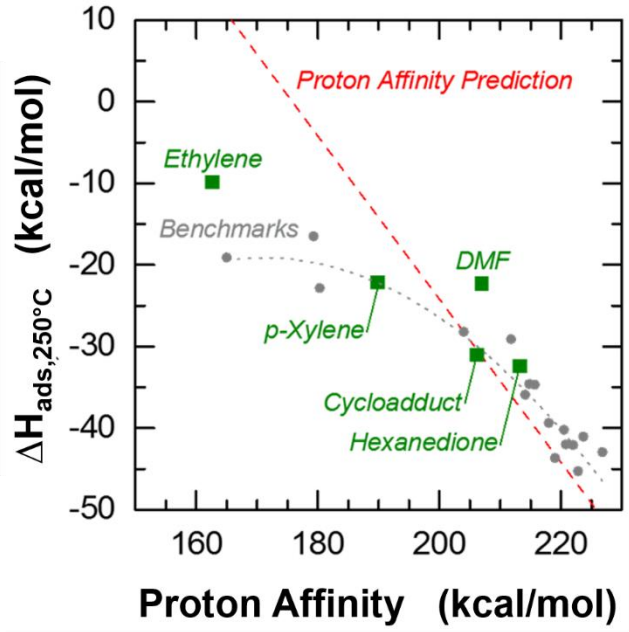

Figure 8. Heat of Adsorption versus Proton Affinity in H-Y Zeolite. Heat of adsorption correlates linearly with proton affinity above 200 kcal/mol. Deviation from the linear proton affinity prediction exists below 200 kcal/mol.

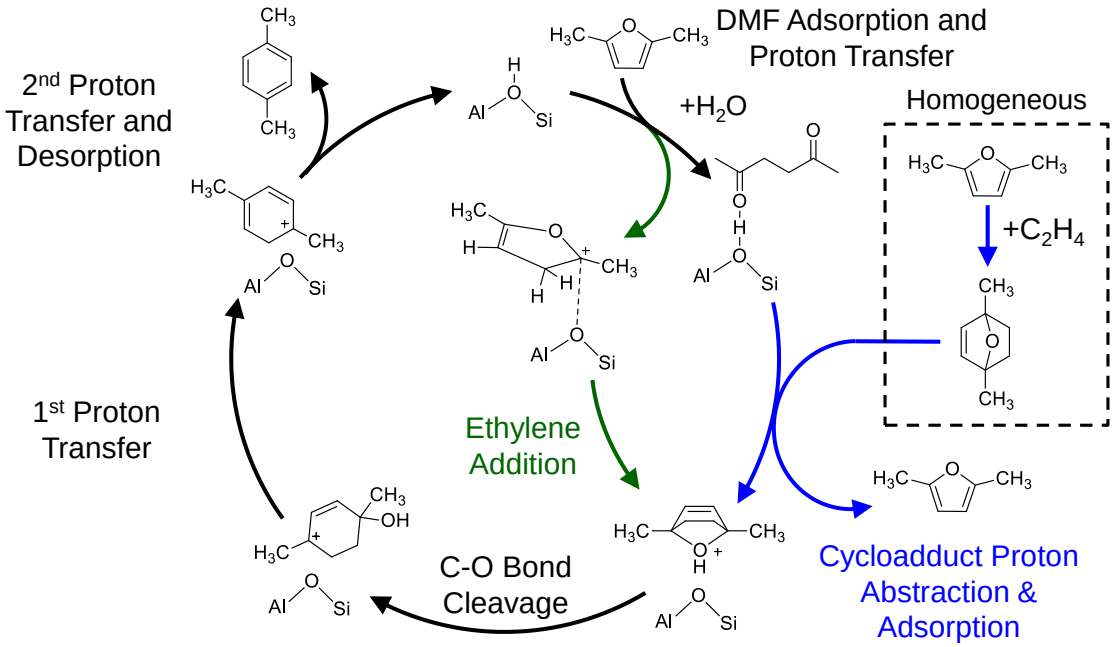

Figure 9. Proposed Catalytic Cycles Converting Dimethylfuran to *p*-Xylene. Brønsted-acid sites within H-BEA and H-Y zeolite catalyze conversion of DMF and ethylene to *p*-xylene and water. Initial high concentration of dimethylfuran (DMF) results in strong adsorption with proton transfer to the α-C or β-C of DMF. High surface coverage of adsorbed DMF blocks Brønsted acid sites, preventing *p*-xylene isomerization reactions. Loss of the aromaticity (and diene character) on adsorption prevents reaction of ethylene by Diels-Alder addition with adsorbed furan (green mechanisms – ethylene addition). Alternatively, DMF reacts with ethylene homogeneously to form a DA cycloadduct, which then replaces adsorbed DMF by proton abstraction or competitive adsorption. Subsequent C-O cleavage, proton transfer and desorption produces *p*-xylene and water and completes the cycle.

Table 1. Characterization of Zeolite Catalysts H-Y (Si/Al 2.6) and H-BEA (Si/Al 12.5).

Catalyst	Preparation Method	Brønsted acid sites (mmol/g)[A]
H-Y (CBV600)	Fresh	0.34 ± 0.04
H-Y (CBV600)	Post-Reaction, Calcined in Air at 550 °C[B]	0.29 ± 0.01
H-Y (CBV600)	DMF-Adsorbed[C]	0.18 ± 0.02
H-BEA (CP814E)	Fresh	0.64 ± 0.03
H-BEA (CP814E)	Post-Reaction, Calcined in Air at 550 °C[B]	0.39 ± 0.01
H-BEA (CP814E)	DMF-Adsorbed[C]	0.42 ± 0.00

[A]Obtained using Isopropylamine-TGA TPD
[B]Obtained following reaction of DMF+C_2H_4 at 300 °C. Calcined in air at 550 °C.
[C]Adsorbed with DMF at 120 °C and then heated to 300 °C for one hour before using standard Isopropylamine-TGA TPD

Table 2. Enthalpies and Gibbs Free Energies of Binding to the H-Y Active Site, in kcal/mol. The markings (P) and (T) denote different adsorption configurations. In geometry (P), the adsorbed molecules are stacked with their molecular planes parallel to the plane of the H-Y Site II hexagonal prism plane; in geometry (T) they are arranged perpendicularly.

Molecule	ΔH_{ads}			ΔG_{ads}		
	200 °C	**250 °C**	**300 °C**	**200 °C**	**250 °C**	**300 °C**
Ethylene[1]	-9.7	-9.6	-9.4	1.7	2.9	4.1
Heptane	-16.1	-15.9	-15.7	0.6	2.4	4.1
Water[1]	-14.7	-14.6	-14.5	-1.9	-0.5	0.8
p-Xylene[1]	-21.6	-21.4	-21.3	-4.0	-2.1	-0.3
DMF[1]	-21.7	-21.5	-21.4	-5.4	-3.6	-1.9
Hexanedione[1]	-30.3	-30.2	-30.0	-12.3	-10.4	-8.5
Oxanorbornene[2]	-30.3	-30.2	-30.0	-13.3	-11.5	-9.7
DMF-DMF (P)	-37.9	-37.6	-37.2	-10.1	-7.2	-4.3
DMF-DMF (T)	-31.4	-31.0	-30.7	-2.3	0.7	3.7
DMF-*p*-xylene (P)	-39.9	-39.5	-39.2	-7.8	-4.5	-1.1
p-xylene-DMF (P)	-37.2	-36.8	-36.5	-10.9	-8.1	-5.4
DMF-*p*-xylene (T)	-35.2	-34.9	-34.5	-2.4	1.0	4.5

Table 3. Enthalpies and Free Energies of Active Site Proton Transfer, in kcal/mol.

Proton Origin	Proton Destination	$\Delta H_{activation}$	$\Delta H_{reaction}$	$\Delta G_{activation}$	$\Delta G_{reaction}$
H-Y	DMF α-Carbon	6.0	-2.3	6.3	-2.9
H-Y	DMF β-Carbon	5.1	0.2	7.8	2.2
H-Y	*p*-Xylene	16.2	15.2	18	16.7
DMF α-Carbon	DMF β-Carbon	16.2	-3.6	16.2	-3.3
DMF β-Carbon	Cycloadduct O	6.6	8.1	8.0	9.0
DMF β-Carbon	*p*-Xylene	25.0	26.0	26.6	27.6

References

[1] Ragauskas, A. J.; Williams, C. K.; Davison, B. H.; Britovsek, G.; Cairney, J.; Eckert, C. A.; Frederick, W. J.; Hallett, J. P.; Leak, D. J.; Liotta, C. L.; Mielenz, J. R.; Murphy, R.; Templer, R.; Tschaplinski, T. *Science* **2006**, *311*, 484−489.

[2] Bridgwater, A. V. *Chem. Eng. J.* **2003**, *91*, 87–102.

[3] Schmidt, L. D.; Dauenhauer, P. J. *Nature* **2007**, *447*, 914–915.

[4] Tong, X.; Ma, Y.; Li, Y. *Appl. Catal. A Gen.* **2010**, *385*, 1–13.

[5] Vlachos, D. G.; Chen, J. G.; Gorte, R. J.; Huber, G. W.; Tsapatsis, M. *Catal. Letters* **2010**, *140*, 77–84.

[6] Partenheimer, W. *Catal. Today* **1995**, *23*, 69–158.

[7] Tsai, T.; Liu, S.; Wang, I. *Appl. Catal. A Gen.* **1999**, *181*, 355–398.

[8] Vispute, T. P.; Zhang, H.; Sanna, A.; Xiao, R.; Huber, G. W. *Science* **2010**, *330*, 1222–7.

[9] Lima, S.; Dias, A. S.; Lin, Z.; Brandão, P.; Ferreira, P.; Pillinger, M.; Rocha, J.; Calvino-Casilda, V.; Valente, A. A. *Appl. Catal. A Gen.* **2008**, *339*, 21–27.

[10] Moliner, M.; Román-Leshkov, Y.; Davis, M. E. *Proc. Natl. Acad. Sci. U. S. A.* **2010**, *107*, 6164–8.

[11] Román-Leshkov, Y.; Chheda, J. N.; Dumesic, J. A. *Science* **2006**, *312*, 1933–1937.

[12] Román-Leshkov, Y.; Barrett, C. J.; Liu, Z. Y.; Dumesic, J. A. *Nature* **2007**, *447*, 982–985

[13] Brandvold, T. A. Carbohydrate Route to p-Xylene and Terephthalic Acid, US Patent 20,100,331,568, December 30, 2010.

[14] Do, P. T. M.; McAtee, J. R.; Watson, D. A.; Lobo, R. F. *ACS Catal.* **2013**, *3*, 41–46.

[15] Nikbin, N.; Do, P. T.; Caratzoulas, S.; Lobo, R. F.; Dauenhauer, P. J.; Vlachos, D. G. *J. Catal.* **2013**, *297*, 35–43.

[16] Nikbin, N.; Feng, S.; Caratzoulas, S.; Vlachos, D. G. *J. Phys. Chem. C* **2014**, *118*, 24415-24424.

[17] M. O. Kusak. Method for adding special elements to molten pig iron, U.S. Patent. 3,833,361, September 3 1974.

[18] Gendy, T. S. *J. Chem. Technol. Biotechnol.* **1998**, *73*, 109–118.

[19] Guisnet, M.; Gnep, N. S.; Morin, S. *Microporous Mesoporous Mater.* **2000**, *35-36*, 47–59.

[20] Corma, A.; Sastre, E. *J. Catal.* **1991**, *129*, 177–185.

[21] S. Morin, N. S. Gnep, and M. Guisnet, *J. Catal.*, 1996, **159**, 296–304

[22] Menezes, S. M. C.; Camorim, V. L.; Lam, Y. L.; San Gil, R. A. S.; Bailly, A.; Amoureux, J. P. *Appl. Catal. A Gen.*, **2001**, *207*, 367–377.

[23] Montanari, T.; Finocchio, E.; Busca, G. *J. Phys. Chem.* **2011**, *115*, 937–943.

[24] Li, S.; Zheng, A.; Su, Y.; Zhang, H.; Chen, L.; Yang, J.; Ye, C.; Deng, F. *J. Am. Chem. Soc.* **2007**, *129*, 11161–71.

[25] Freude, D.; Ernst, H.; Wolf, I. *Solid State Nucl. Magn. Reson.* **1994**, *3*, 271–86.

[26] Remy, M. J.; Stanica, D.; Poncelet, G.; Feijen, E. J. P.; Grobet, P. J.; Martens, J. A. *J. Phys. Chem.* **1996**, *100*, 12440–12447.

[27] Green, S. K.; Patet, R. E.; Nikbin, N.; Williams, C. L.; Chang, C-C.; Yu, J.; Gorte, R. J.; Caratzoulas, S.; Fan, W.; Vlachos, D. G.; Dauenhauer, P. J. *Appl. Catal., B* **2015**, *180*, 487-496.

[28] Svensson, M.; Humbel, S.; Froese, R. D. J.; Matsubara, T.; Sieber, S.; Morokuma, K. *J. Phys. Chem.* **1996**, *100*, 19357–19363.

[29] Frisch, M. J.; Trucks, G. W.; Schlegel, H. B.; Scuseria, G. E.; Robb, M. A.; Cheeseman, J. R.; Scalmani, G.; Barone, V.; Mennucci, B.; Petersson, G. A.; Nakatsuji, H.; Caricato, M.; Li, X.; Hratchian, H. P.; Izmaylov, A. F.; Bloino, J.; Zheng, G.; Sonnenberg, J. L.; Hada, M.; Ehara, M.; Toyota, K.; Fukuda, R.; Hasegawa, J.; Ishida, M.; Nakajima, T.; Honda, Y.; Kitao, O.; Nakai, H.; Vreven, T.; Montgomery, J. A., Jr.; Peralta, J. E.; Ogliaro, F.; Bearpark, M.; Heyd, J. J.; Brothers, E.; Kudin, K. N.; Staroverov, V. N.; Kobayashi, R.; Normand, J.; Raghavachari, K.; Rendell, A.; Burant, J. C.; Iyengar, S. S.; Tomasi, J.; Cossi, M.; Rega, N.; Millam, N. J.; Klene, M.; Knox, J. E.; Cross, J. B.; Bakken, V.; Adamo, C.; Jaramillo, J.; Gomperts, R.; Stratmann, R. E.; Yazyev, O.; Austin, A. J.; Cammi, R.; Pomelli, C.; Ochterski, J. W.; Martin, R. L.; Morokuma, K.; Zakrzewski, V. G.; Voth, G. A.; Salvador, P.;

Dannenberg, J. J.; Dapprich, S.; Daniels, A. D.; Farkas, Ö.; Foresman, J. B.; Ortiz, J. V.; Cioslowski, J.; Fox, D. J. *Gaussian09*; Gaussian, Inc.: Wallingford CT, 2009.
[30] Zhao, Y.; Truhlar, D. G.; *Theor. Chem. Acc.* **2007**, *120*, 215–241.
[31] Dessau, R. M.; *Zeolites* **1990**, *10*, 205–206.
[32] Beyerlein, R. A.; Choi-feng, C.; Hall, J. B.; Huggins, B. J.; Ray, G. J. *Top. Catal.* **1997**, *4*, 27–42.
[33] Gorte, R. J. *Catal. Lett.* **1999**, *62*, 1-13.
[34] Solans-Monfort, X., Sodupe, M., Mó, O., Yáñez, M., Elguero, J., *J. Phys. Chem. B*, **2005**, *109*, 19301-19308.
[35] Vaitheeswaran, S.; Green, S. K.; Dauenhauer, P. J.; Auerbach, S. M. *ACS Catal.* **2013**, *3*, 2012–2019.
[36] Patet, R. E.; Nikbin, N.; Williams, C. L.; Green, S. K.; Chang, C.-C.; Fan, W.; Caratzoulas, S.; Dauenhauer, P. J.; Vlachos, D. G. *ACS Catal.* **2015**, *5*, 2367-2375.
[37] Green, S. K.; Patet, R. E.; Nikbin, N.; Williams, C. L.; Chang, C.-C.; Yu, J.; Gorte, R. J.; Caratzoulas, S.; Fan, W.; Vlachos, D. G.; Dauenhauer, P. J. *Appl. Catal. B* **2015**, *180*, 487-496.
[38] Nikbin, N.; Caratzoulas, S.; Vlachos, D. G. *ChemSusChem* **2013**, *6*, 2066–8.
[50] Kiricsi, I.; Flego, C.; Pazzuconi, G.; Parker, W. J.; Millini, R.; Perego, C.; Bellussi, G. *J. Phys. Chem.* **1994**, *98*, 4627-4634.